Original Research Article

International journal of spray and combustion dynamics

International Journal of Spray and Combustion Dynamics
2018, Vol. 10(4) 326–336

DOI: 10.1177/1756827718809570
journals.sagepub.com/home/scd
SAGE

Analysis of the interaction of thermoacoustic modes with a Green's function approach

Alessandra Bigongiari[1,2] and Maria Heckl[1]

Abstract

In this paper, we will present a fast prediction tool based on a one-dimensional Green's function approach that can be used to bypass numerically expensive computational fluid dynamics simulations. The Green's function approach has the advantage of providing a clear picture of the physics behind the generation and evolution of combustion instabilities. In addition, the method allows us to perform a modal analysis; single acoustic modes can be treated in isolation or in combination with other modes. In this article, we will investigate the role of higher-order modes in determining the stability of the system. We will initially produce the stability maps for the first and second mode separately. Then the time history of the perturbation will be computed, where both the modes are present. The flame will be modelled by a generic Flame Describing Function, i.e. by an amplitude-dependent Flame Transfer Function. The time-history calculations show the evolution of the two modes resulting from an initial perturbation; both transient and limit-cycle oscillations are revealed. Our study represents a first step towards the modelling of nonlinearity and non-normality in combustion processes.

Keywords

Non-normality, nonlinearity, thermoacoustic instability, Green's function, heat release model, flame describing function, network model, distributed time-lags, thermoacoustic feedback

Date received: 18 May 2018; accepted: 8 October 2018

1. Introduction

Thermoacoustic instabilities are large-amplitude self-sustained oscillations of the acoustic field that are observed in various combustion systems.[1,2] They arise as the result of thermoacoustic feedback, i.e. positive feedback between the heat source (typically a flame) and the acoustic field inside the combustor. What starts as a small perturbation in the acoustic field amplifies the rate of heat release, which in turn amplifies the acoustic field; this process is repeated periodically, and high amplitudes are soon reached. Whether the feedback is positive depends on the system parameters. It may also be negative, in which case an initial perturbation decays. Efforts have been made by several research groups to understand and control this phenomenon. One can get an overview in the review articles of Candel,[3] Lieuwen[4] and Huang and Yang,[5] in the books by Lieuwen and Yang[6] and Poinsot and Veynante,[7] and in Culick.[8]

Several unstable thermoacoustic modes may appear simultaneously in a combustion system. Some modes are more harmful that others, so it is important to predict their frequency and amplitude, and to understand the interaction between them. The aim of this paper is to present a fundamental study of a two-mode combustion system in order to shed light on the behaviour of the individual modes and on the interaction between them.

There are only a few fundamental studies of nonlinear modal interactions in the literature.

Moeck et al[9] performed a frequency-domain study of modal interactions by the "harmonic balance approach". Starting from a nonlinear heat release law in the time-domain, they constructed a multi-input FDF. They then incorporated this FDF into a network model in the frequency domain and derived a *set* of dispersion relations. These have the form of coupled nonlinear algebraic equations for the frequencies and

[1]School of Chemical and Physical Sciences, Keele University, Staffordshire, UK
[2]Dipartimento di Fisica, Università di Pisa, Pisa, Italy

Corresponding author:
Maria Heckl, School of Chemical and Physical Sciences, Keele University, Staffordshire ST5 5BG, UK.
Email: m.a.heckl@keele.ac.uk

amplitudes of the individual modes. Any modes participating in a limit cycle were identified from their purely real eigenfrequencies and corresponding non-zero amplitudes. The method is suitable for the case where only two modes are involved in the interaction, but becomes excessively laborious if there are more than two modes. Also, it provides information only on established limit cycles oscillations, but not on any transient states.

Acharya et al[10] studied modal interactions for the special case, where there are two potentially unstable modes, which have *similar frequencies*. Their study is based on the nonlinear wave equation for the pressure with a forcing term that is proportional to the rate of heat release. The heat release rate is assumed to depend on pressure (not on velocity) and described by a cubic expression. The Galerkin method is used to formulate ODEs for the time dependence of the two modes; they have the form of coupled oscillator equations with nonlinear "forcing terms". Since the frequency difference between the two modes is assumed to be small, a slow time-scale occurs in addition to the fast time-scale related to the oscillation frequencies. The presence of two time scales allows the use of the "method of averaging", i.e. simplifying the coupled oscillator equations by neglecting the time averages of the fast variations. The averaged equations are analysed to predict the limit cycle amplitudes of the two modes for a range of parameters. The method is limited to modes with similar frequencies and cannot be extended to other frequencies.

Another time-domain study was performed by Noiray et al[11] for azimuthal modes in an annular combustion chamber. They considered the interaction between a pair of azimuthal modes with the same mode number. As in[10], the heat release rate was modelled by a cubic expression in terms of the acoustic pressure. A pair of coupled ODEs was formulated for the temporal evolution of the amplitudes of the two modes. These ODEs turned out to represent a pair of coupled Van der Pol oscillators. The mode pair was found to be able to form a limit cycle, and their nature (rotating, standing, or mixed) was determined for different azimuthal distributions of the heat release rate. This method can only be applied to the special case where two modes with the same frequency interact.

Our approach is primarily in the time-domain and analytical. It differs from the studies referenced above in two main aspects:

- We use the tailored Green's function to describe the acoustic field in the combustion chamber; we do *not* use the Galerkin method, which is commonly used for analytical studies in thermoacoustics (e.g. in[9-14]).
- We model the nonlinear flame by a generic analytical heat release law with amplitude-dependent fitting parameters that can be adjusted to capture the typical features of any given flame describing function; we do *not* assume a priori that the heat release depends on the acoustic field in a specific nonlinear fashion, and we do *not* impose an a priori saturation amplitude.

The tailored Green's function is a superposition of modes of the combustion system without feedback. We calculate its modal frequencies, growth rates and amplitudes in terms of a few key parameters, such as combustor geometry, end conditions, inlet and outlet temperature. We then use the Green's function to derive a governing equation for the combustion system *with* feedback. This equation captures the key physical aspects: the combustor properties and the parameters describing the thermoacoustic feedback.

Our method has a number of advantages over the earlier methods.

- It is not limited to two modes, but can be extended to three or more modes in a straightforward way.
- Given that it is a time-domain method, it predicts the behaviour of the interacting modes not only during a limit cycle, but also during transient stages.
- The flame model we use is flexible and can be matched to flame describing functions that are typically found by measurement or by combustion CFD.
- Since our analysis is based on the tailored Green's function of the combustion chamber, our representation of the thermoacoustic field is an expansion in terms of actual physical modes (as opposed to the *approximate* modes of the commonly used Galerkin method). Thus we have a natural and tool to study the interaction of such modes.
- It allows one to make stability predictions quickly and without much numerical effort.

Our method has been described in Bigongiari and Heckl,[15] where the stability of the first acoustic mode has been analysed for two burner configurations: a

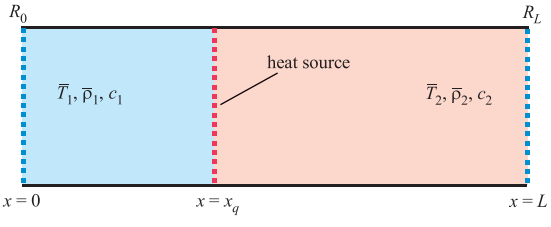

Figure 1. Schematic illustration of the modelled configuration. R_0 and R_L are reflection coefficients. $\bar{T}_1, \bar{\rho}_1, c_1$ are the mean temperature, mean density and speed of sound, respectively in the cold region; $\bar{T}_2, \bar{\rho}_2, c_2$ are their equivalents in the hot region.

Rijke tube and a quarter-wave resonator. In the current paper, we will investigate the role of higher modes in determining the stability behaviour of the system.

Since this is a fundamental study, we consider a simplified combustion system with two main components:

1. The combustion chamber is either a Rijke tube or a quarter-wave resonator. The first two modes are present, but higher modes do not exist.
2. The heat release rate is described by a generic flame describing function (FDF). It is analytical and includes time-lag distributions with amplitude-dependent parameters. Despite its generic nature, it has a realistic basis: it comes from full 3D simulations of a specific laboratory swirl burner (the 'BRS (Beschaufelter Ring-Spalt) burner'),[16] as reported in Iurashev et al.[17] and Bigongiari and Heckl.[18,19]

The paper is organized as follows. The tailored Green's function is introduced in section 2, and its analytical form is given in terms of a superposition of modes. In section 3, we present our model for the heat release rate, both in the time domain and in the frequency domain. The stability analysis is performed in two ways: by calculating the time evolution of an initial perturbation (section 4) and by a modal stability analysis (section 5). Results predicted from the two methods are shown and compared in section 6. The paper finishes with conclusions in section 7.

2. Green's function for the combustion system

We consider the configuration shown in Figure 1. A 1D tube of length L has boundary conditions described by pressure reflection coefficients R_0 and R_L. A steady heat source at x_q creates a mean temperature jump from $\bar{T}_1$ to $\bar{T}_2$, and associated jumps in the mean density $\bar{\rho}$ and speed of sound c. Conditions are uniform within the cold region $0 < x < x_q$ (denoted by subscript 1) and the hot region $x_q < x < L$ (denoted by subscript 2).

The Green's function is the acoustic field generated in the tube at location x and time t by an impulsive point source located at x' and firing at t'. We denote it by $G(x, x', t, t')$ and describe it in terms of the velocity potential. Its governing equation is the non-homogeneous wave equation

$$\frac{1}{c^2}\frac{\partial^2 G}{\partial t^2} - \frac{\partial^2 G}{\partial x^2} = \delta(x - x')\delta(t - t') \tag{1}$$

together with boundary conditions described by reflection coefficients R_0 and R_L. The Green's function is a superposition of modes, with modal amplitudes g_n and modal frequencies ω_n

$$G(x, x', t, t') = H(t - t')\Re\sum_{n=1}^{\infty} g_n(x, x')e^{-i\omega_n(t-t')} \tag{2}$$

$H(t - t')$ denotes the Heaviside function; it guarantees causality. The quantities g_n and ω_n have been calculated analytically for the combustion system shown in Figure 1 (see Bigongiari and Heckl[15] for details on the derivation); the results are

$$g_n(x, x') = i\frac{\hat{g}(x, x', \omega_n)}{\omega_n F(\omega_n)} \tag{3}$$

with

$$\hat{g}(x, x', \omega) = \begin{cases} D(x, \omega)C(x', \omega) & \text{for} \quad x_q < x < x' \\ C(x, \omega)D(x', \omega) & \text{for} \quad x' < x < L \end{cases} \tag{4}$$

and

$$C(x, \omega) = e^{\frac{i\omega}{c_2}(x-L)} + R_L e^{-\frac{i\omega}{c_2}(x-L)} \tag{5a}$$

$$D(x, \omega) = \frac{1}{2}\frac{c_2}{c_1}\left(R_0 \mathrm{e}^{\mathrm{i}\omega\frac{xq}{c1}} - \mathrm{e}^{-\mathrm{i}\omega\frac{xq}{c1}}\right)\left(\mathrm{e}^{\mathrm{i}\frac{\omega}{c2}(x-xq)} - \mathrm{e}^{-\mathrm{i}\frac{\omega}{c2}(x-xq)}\right) + \frac{1}{2}\frac{\bar{\rho}_1}{\bar{\rho}_2}\left(R_0 \mathrm{e}^{i\omega\frac{xq}{c1}} + \mathrm{e}^{-i\omega\frac{xq}{c1}}\right)\left(\mathrm{e}^{\frac{i\omega}{c2}(x-xq)} + \mathrm{e}^{-i\frac{\omega}{c2}(x-xq)}\right) \tag{5b}$$

$$F(\omega) = \frac{1}{2}\frac{1}{c_1}\left[i\left(R_0 e^{i\omega\frac{xq}{c1}} - e^{-i\omega\frac{xq}{c1}}\right)\left(e^{i\omega\frac{xq-L}{c2}} + R_L e^{-i\omega\frac{xq-L}{c2}}\right) - i\frac{c_1}{c_2}\frac{\bar{\rho}_1}{\bar{\rho}_2}\left(e^{i\omega\frac{xq-L}{c2}} - R_L e^{-i\omega\frac{xq-L}{c2}}\right)\left(R_0 e^{i\omega\frac{xq}{c1}} + e^{-i\omega\frac{xq}{c1}}\right)\right] \tag{6}$$

$F(\omega)$ is the function appearing in the characteristic equation, $F(\omega) = 0$, which determines the modal frequencies ω_n in the Green's function.

3. Model for the heat release rate

3.1 Heat release law in the time domain

We construct a heat release law for a compact heat source, which is an extension of the well-known $n\tau$-law. It features distributions around two central time-lag values τ_1 and τ_2, two coupling coefficients n_1 and n_2, as well as the parameters σ_1 and σ_2, which specify the width of the distributions[20]

$$\frac{Q(t)}{\bar{Q}} = n_1\int_{\tau=0}^{\infty}\frac{u_q(t-\tau)}{\bar{U}}D_1(\tau - \tau_1)\mathrm{d}\tau - n_2\int_{\tau=0}^{\infty}\frac{u_q(t-\tau)}{\bar{U}}D_2(\tau - \tau_2)\mathrm{d}\tau \tag{7}$$

Q is the fluctuation of the heat release rate, u_q is the velocity perturbation at the heat source, and $\bar{Q}$ and $\bar{U}$ are the corresponding mean quantities. The

distributions are assumed to be Gaussian with standard deviations σ_1 and σ_2

$$D_i(\tau) = \frac{2}{\sigma_i\sqrt{2\pi}} e^{-\frac{(\tau-\tau_i)^2}{2\sigma_i^2}}, \quad i = 1, 2 \tag{8}$$

The heat release law described by equation (7) includes the $n\tau$-law as special case ($n_2 = 0$, $D_1(\tau - \tau_1) = \delta(\tau - \tau_1)$), but it is much more versatile and able to capture a variety of physical effects:

1. Heat release fluctuations may be induced by different physical effects, such as fluctuations in equivalence ratio, or vortex shedding at the flame holder. Such perturbations may travel with different speeds or over different distances, giving rise to two distinct time-lags in the flame response.
2. Neighbouring fluid particles may travel over slightly different distances and reach the flame front with slightly different travel times. This is included in our model by incorporating the distributions D_1 and D_2.

Based on equation (7) the local heat release rate (per unit mass) can be written as

$$q(t) = K\left[n_1 \int_{\tau=0}^{\infty} u_q(t-\tau) D_1(\tau - \tau_1) \mathrm{d}\tau - n_2 \int_{\tau=0}^{\infty} u_q(t-\tau) D_2(\tau - \tau_2) \mathrm{d}\tau\right] \tag{9}$$

where

$$K = \frac{\bar{Q}}{S\bar{U}_2\bar{\rho}_2} \tag{10}$$

is the heater power per mass flow, having units Wskg^{-1}; S is the cross-sectional area of the tube.

The time-lags τ_1, τ_2, the coupling constants n_1, n_2, and the distribution widths σ_1, σ_2, are all amplitude-dependent. The inclusion of the amplitude-dependence is fundamental to the modelling of non-linear effects, such as the formation of limit cycles. In order to determine the amplitude-dependence, we are going to move from the time-domain to the frequency-domain.

3.2 Heat release law in the frequency domain

We denote the Fourier transform by $\mathcal{F}[\,]$ and Fourier-transformed quantities by $\hat{}$, e.g.

$$\mathcal{F}[Q(t)] = \frac{1}{2\pi} \int_{t=-\infty}^{\infty} Q(t) e^{i\omega t} \mathrm{d}t = \hat{Q}(\omega) \tag{11}$$

Assuming that the distribution is zero for negative time-lags, i.e. $D_i(\tau - \tau_i) = 0$ for $\tau \leq 0$, we can extend the range of integration from $[0, \infty]$ to $[-\infty, \infty]$ and calculate the Fourier transform of equation (7)

$$\frac{\hat{Q}(\omega)}{Q} = n_1 \frac{\hat{u}_q}{\bar{U}} e^{i\omega\tau_1} e^{-\sigma_1^2\omega^2/2} - n_2 \frac{\hat{u}_q}{\bar{U}} e^{i\omega\tau_2} e^{-\sigma_1^2\omega^2/2} \tag{12}$$

This gives the flame transfer function

$$\mathrm{FTF}(\omega) = \frac{\hat{Q}(\omega)/\bar{Q}}{\hat{u}_q(\omega)/\bar{U}} = n_1 e^{i\omega\tau_1} e^{-\sigma_1^2\omega^2/2} - n_2 e^{i\omega\tau_2} e^{-\sigma_2^2\omega^2/2} \tag{13}$$

where $\hat{Q}$ and $\hat{u}_q$ are the fluctuations in the frequency domain of the heat release rate and velocity, respectively. The FTF in equation (13) shows the same key features that are generally observed in FTF measurements of premixed flames, as shown in Bigongiari and Heckl,[19] in particular the excess gain and the low-pass behaviour.

Since we assume that the parameters n_1, n_2, τ_1, τ_2, σ_1, σ_2 are amplitude-dependent, the FTF in equation (13) is amplitude-dependent. In other words, it is a 'flame describing function', which is commonly defined by

$$\mathrm{FDF}(A, \omega) = \frac{\hat{Q}(A, \omega)/\bar{Q}}{\hat{u}_q(A, \omega)/\bar{U}} \tag{14}$$

the letter A denotes the velocity amplitude (at the heat source).

The FDF can be determined experimentally by applying a harmonic perturbation at the inlet (usually through a loudspeaker or a siren) and recording the time histories of the acoustic velocity and heat release rate fluctuations. Spectral analysis then allows the calculation of the gain and phase of the FTF as a function of frequency and perturbation amplitude (see Noiray et al.[21]). This experimental procedure can be mimicked by full CFD simulations, as shown in Iurashev et al.[17]

In order to work with realistic values for n_1, n_2, τ_1, τ_2, σ_1, σ_2, we are going to choose them by treating them as fitting parameters and matching equation (13) to the FTF in Iurashev et al.,[17] which comes from CFD simulations of the BRS burner. This is done for four amplitude values in the range [0, 0.31] and leads to amplitude-dependent fitting parameters n_1, n_2, τ_1, τ_2, σ_1, σ_2. We describe the amplitude-dependence analytically by the following linear expressions (for details see Bigongiari and Heckl[19])

$$n_1 = 7.4 - 14.94\frac{A}{\bar{U}}, \quad n_2 = 4.7 - 14.94\frac{A}{\bar{U}} \tag{15}$$

$$\tau_1 = 4.13 - 6.56\frac{A}{\bar{U}}, [ms], \quad \tau_2 = 6.31 - 1.89\frac{A}{\bar{U}}, [ms] \tag{16}$$

$$\sigma_1 = 1.94 - 3.16\frac{A}{\bar{U}}, [ms], \quad \sigma_2 = 1.21 - 1.54\frac{A}{\bar{U}}, [ms] \tag{17}$$

This approach to modelling amplitude-dependent heat release laws represents an advance over early nonlinear models, where an artificial saturation amplitude was imposed in order to 'predict' limit cycles.[22] Further details about nonlinear analytical flame models of the sort described in this section can be found in[20], where they were first published.

4. Time evolution

4.1 The integral governing equation

In this section, we derive a time-domain expression for the acoustic field in the burner in terms of its Green's function and the heat release rate.

The velocity potential $\phi(x,t)$ of a sound field generated by a heat source with heat release rate $q(x,t)$ (per unit mass) can be described by the acoustic analogy equation

$$\frac{1}{c^2}\frac{\partial^2\phi}{\partial t^2}-\frac{\partial^2\phi}{\partial x^2}=-\frac{\gamma-1}{c^2}q(x,t) \tag{18}$$

together with the initial conditions

$$\phi(x,t)\big|_{t=o}=\varphi_0\delta\big(x-x_q\big) \text{ and } \left.\frac{\partial\phi(x,t)}{\partial t}\right|_{t=o}=\varphi_0'\delta\big(x-x_q\big) \tag{19}$$

φ_0 is the initial value of the velocity potential, and φ'_0 is the initial value of its time derivative.

This set of equations can be converted into an integral equation for the acoustic velocity u with the use of the Green's function. For a compact heat source at $x=x_q$, described by

$$q(x,t)=q(t)\delta\big(x-x_q\big) \tag{20}$$

we obtain the following integral equation (for details of the derivation see Heckl and Howe[19])

$$\begin{aligned}u_q(t)=\left.\frac{\partial\phi}{\partial x}\right|_{x=x_q}&=-\frac{\gamma-1}{c^2}\int_{t'=0}^{t}\left.\frac{\partial G(x,x',t,t')}{\partial x}\right|_{\substack{x=x_q\\x'=x_q}}q(t')dt'\\&-\frac{\varphi_0}{c^2}\left.\frac{\partial G}{\partial x\partial t'}\right|_{\substack{x=x_q\\x'=x_q\\t'=0}}+\frac{\varphi_0'}{c^2}\left.\frac{\partial G}{\partial x}\right|_{\substack{x=x_q\\x'=x_q\\t'=0}}\end{aligned} \tag{21}$$

It is worth noting that equation (21) is equivalent to the set of governing equations comprising equations (18) and (19), and the boundary conditions described by R_0 and R_L. In order to close the problem, an expression for $q(t)$ in terms of u_q is required. The equation can then be integrated numerically to obtain the time evolution of the perturbation.

4.2 Numerical solution by iteration

In order to solve equation (21) by iteration, we define the integral

$$I_n(t)=\int_{t'=0}^{t'=t}e^{i\omega_n t'}q(t')\mathrm{d}t' \tag{22}$$

and split it into two parts (one over the slightly reduced time interval $t'=0,\ldots t-\Delta t$ and one over the small time interval $t'=t-\Delta t,\ldots t$)

$$I_n(t)=\int_{t'=0}^{t-\Delta t}e^{i\omega_n t'}q(t')\mathrm{d}t'+\int_{t'=t-\Delta t}^{t}e^{i\omega_n t'}q(t')\mathrm{d}t' \tag{23}$$

We use this, and the modal form of $G(x,x',t,t')$ in equation (2), to rewrite the integral equation (10) as

$$\begin{aligned}u_q(t)=&-\frac{\gamma-1}{c^2}\mathrm{Re}\sum_{n=1}^{\infty}G_n e^{-i\omega_n t}I_n(t)\\&-\frac{1}{c^2}\mathrm{Re}\sum_{n=1}^{\infty}\big(i\omega_n\varphi_0+\varphi_0'\big)G_n e^{-i\omega_n t}\end{aligned} \tag{24}$$

where the abbreviation

$$G_n=\left.\frac{\partial g_n(x,x')}{\partial x}\right|_{\substack{x=x_q\\x'=x_q}} \tag{25}$$

has been introduced. With the assumption that $q(t')$ is constant during the small time interval Δt, the integral I_n can be approximated as

$$I_n(t)=I_n(t-\Delta t)+q(t-\Delta t)\frac{1-e^{-i\omega_n\Delta t}}{i\omega_n}e^{i\omega_n t} \tag{26}$$

The modal frequencies ω_n are obtained by numerical solution (e.g. by the Newton–Raphson method) of the characteristic equation $F(\omega)=0$, with $F(\omega)$ defined in equation (6). In each iteration step, $I_n(t)$ is updated by equation (26), then $u_q(t)$ by equation (24), and finally $q(t)$ by the heat release law equation (9).

5. Modal analysis

The integral equation (21) governs the evolution of the acoustic field in the presence of thermoacoustic feedback. From this equation it is possible to perform a modal analysis resembling an eigenvalue calculation that gives the frequencies of the acoustic modes *driven by thermoacoustic feedback*. The eigenmodes are determined by using a modal expression for the acoustic velocity with complex amplitudes u_m and complex frequencies Ω_m

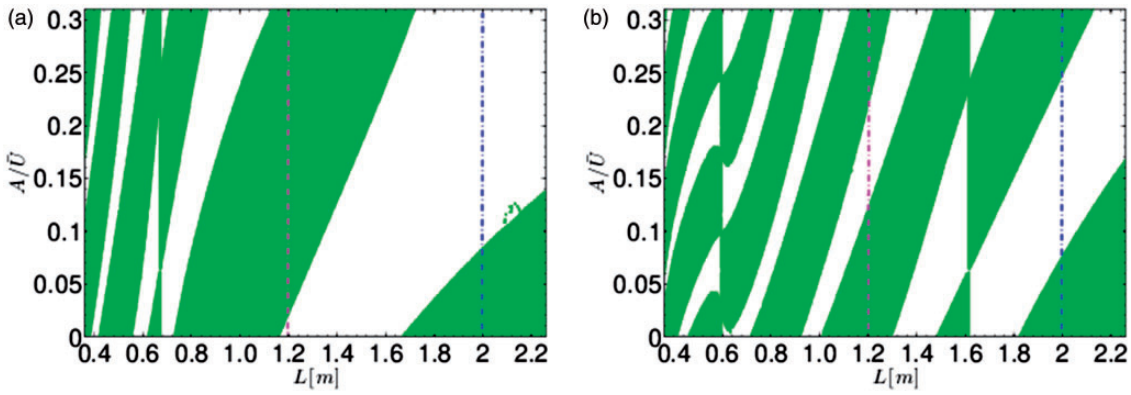

Figure 2. Stability maps in the $L - A/\bar{U}$ plane for a Rijke tube with heat source at $x_q = 0.20$m. The mean temperature jumps from 300K to 1400K. (a) Mode 1 in isolation. (b) Mode 2 in isolation.

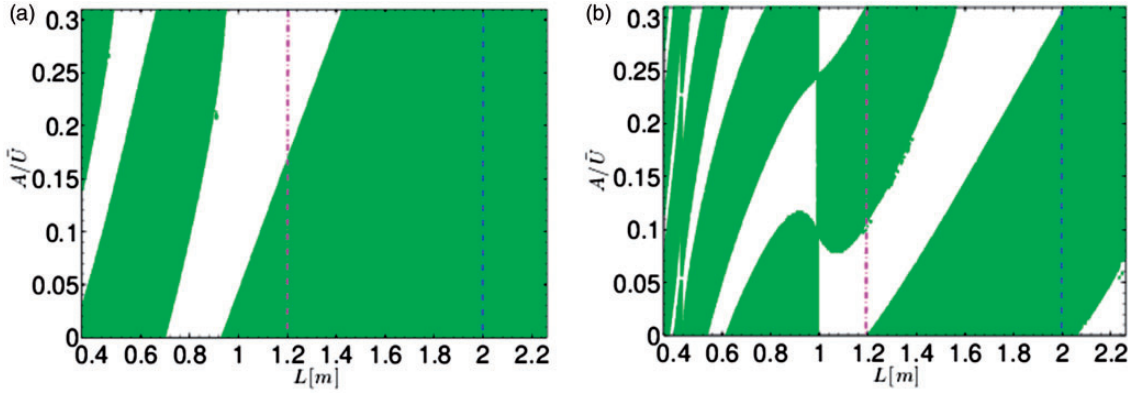

Figure 3. Stability maps in the $L - A/\bar{U}$ plane for a quarter-wave resonator with heat source at $x_q = 0.20$m. The mean temperature jumps from 300K to 1400K. (a) Mode 1 in isolation. (b) Mode 2 in isolation.

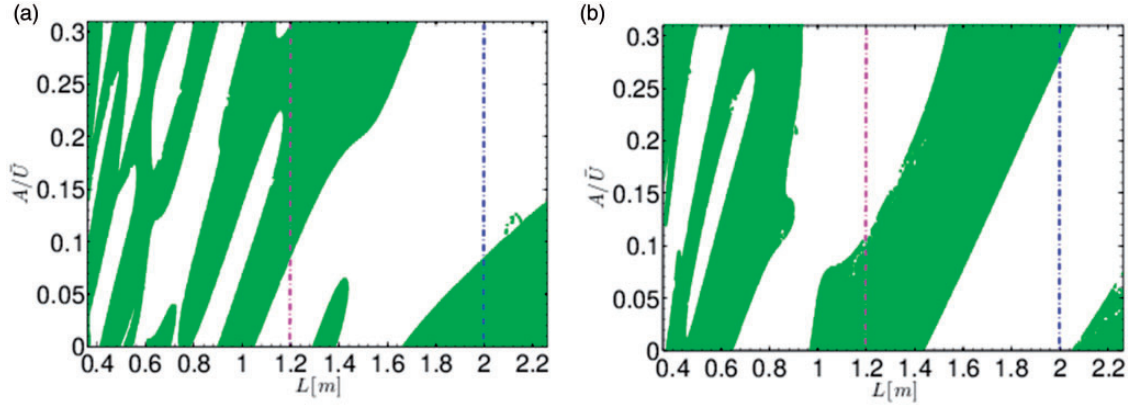

Figure 4. Comparative maps for $\Im(\Omega_1)$ and $\Im(\Omega_2)$. Green areas indicate $\Im(\Omega_1) > \Im(\Omega_2)$. (a) Rijke tube. (b) Quarter-wave resonator. The other parameters are as in figures 2 and 3.

$$u_q(t) = \sum_{m=1}^{\infty} \left(u_m e^{-i\Omega_m t} + u_m^* e^{i\Omega_m^* t} \right) \tag{27}$$

Equations for u_m and Ω_m are derived by combining equation (27) with the integral equation (21), the local heat release rate $q(t)$ in equation (9), and the modal expression for the Green's function in equation (2). We report here the equations for Ω_m obtained in

Bigongiari and Heckl[15] and extended to include the time-lag distribution

$$\int_{\tau=0}^{\infty} e^{i\Omega_m t}[n_1 D_1(\tau) - n_2 D_2(\tau)]\mathrm{d}\tau \times \sum_{n=1}^{\infty}\left[\frac{G_n}{i(\omega_n - \Omega_m)} - \frac{G_n^*}{i(\omega_n^* + \Omega_m)}\right] = -\frac{2c^2}{K(\gamma-1)} \tag{28}$$

with G_n given by equation (25).

By solving equation (27) for Ω_m and then determining the sign of $\Im(\Omega_m)$, the stability behaviour of mode m can be predicted directly. We will perform this kind of stability analysis for different control parameters and perturbation amplitudes, and then represent our predictions in the form of stability maps. This has been done in Bigongiari and Heckl,[15] where the dependence on heater power, heat source position and length of the pipe were analysed *for the first acoustic mode in isolation*.

In this paper, we are going to extend our analysis and concentrate on the effects of higher-order modes on stability, as well as on the interaction between the first and second acoustic mode.

6. Results

In order to study the stability behaviour of the system, we use the two approaches described earlier: we calculate stability maps from a modal analysis as described in section 5, and we calculate perturbation time histories as described in section 4.2. Modes 1 and 2 will be taken into account. The calculations will be performed for two sets of boundary conditions without acoustic losses:

1. $R_0 = 1$ (rigid end at $x = 0$) and $R_L = -1$ (open end at $x = L$), i.e. for a *quarter-wave resonator*.
2. $R_0 = -1$ (open end at $x = 0$) and $R_L = -1$ (open end at $x = L$), i.e. for a *Rijke tube*.

The heater position is kept constant, $x_q = 0.20$ m. The heater power per mass flow is assumed to be $K = 1.41 \times 10^6 \mathrm{Wskg}^{-1}$. The corresponding temperature

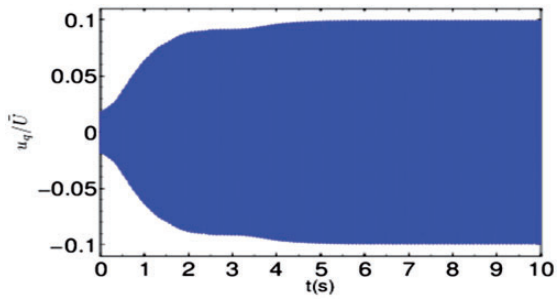

Figure 5. Time history of $u_q(t)$ in a Rijke tube with $L = 1.2$ m and initial condition $u_q(t = 0)/\bar{U} = 0.01$. The Green's function includes the first two modes. $x_q = 0.20$m, $\bar{T}_1 = 300$K, $\bar{T}_2 = 1400$K.

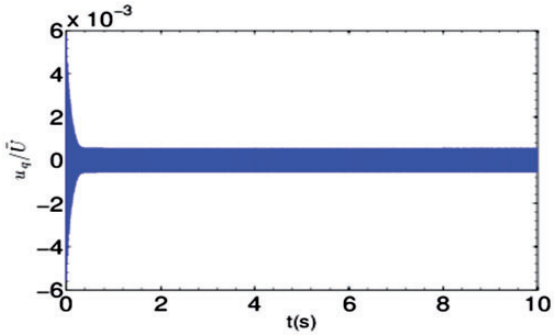

Figure 7. Time history of $u_q(t)$ in a quarter-wave resonator with $L = 2$ m and initial condition $u_q(t = 0)/\bar{U} = 0.01$. The Green's function includes the first two modes. $x_q = 0.20$m, $\bar{T}_1 = 300$K, $\bar{T}_2 = 1400$K.

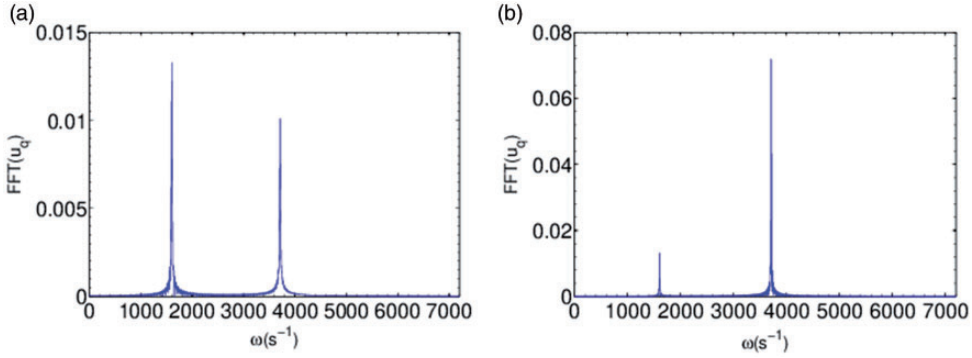

Figure 6. Fourier transform of the time history $u_q(t)$ shown in Figure 5. (a) Time-window [0, 1 s]. (b) Time-window [9 s, 10 s].

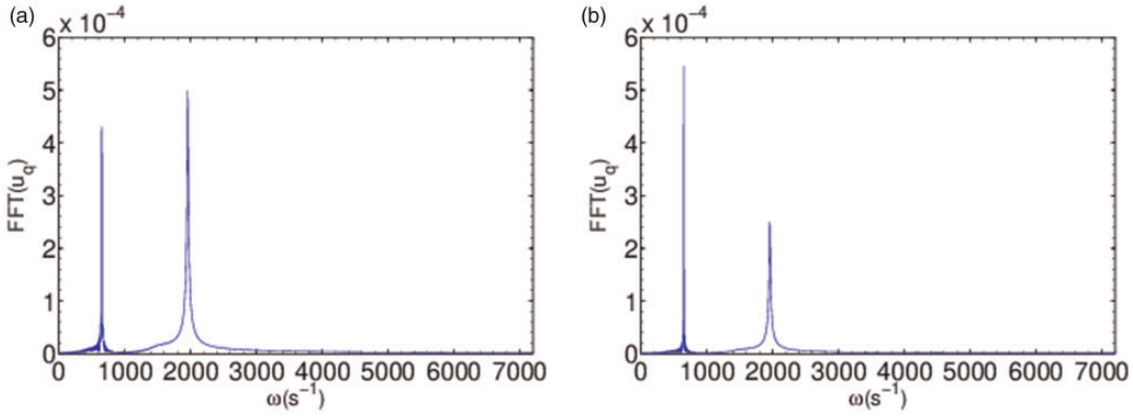

Figure 8. Fourier transform of the time history $u_q(t)$ shown in Figure 7. (a) Time-window [0, 1 s]. (b) Time-window [9 s, 10 s].

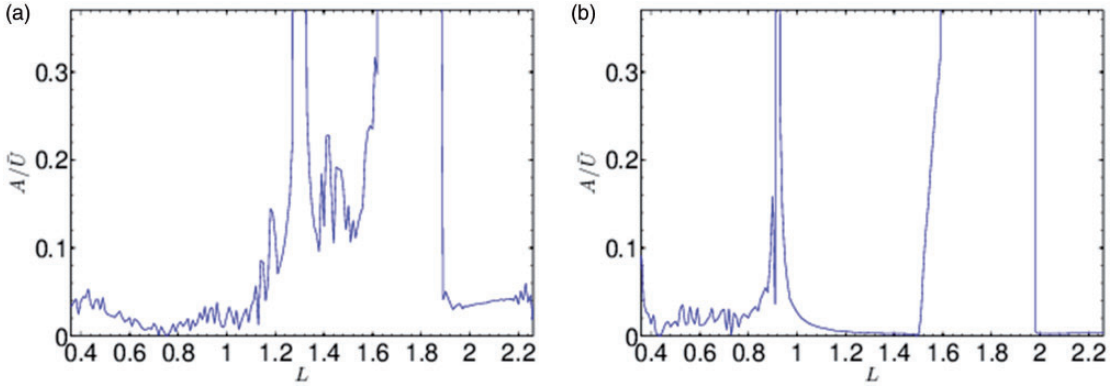

Figure 9. Amplitude of the perturbation after 1s, as a function of the combustor length L. The increment is ΔL=0.01m. $x_q = 0.20$m, $\bar{T}_1 = 300$K, $\bar{T}_2 = 1400$K. (a) Rijke tube. (b) Quarter-wave resonator.

jump is $\Delta T = 1400\,\mathrm{K}$; the inlet temperature is $\bar{T}_1 = 300K$, and the outlet temperature is $\bar{T}_2 = \bar{T}_1 + \Delta T$.

The Green's function is assumed to have only two non-zero modes, i.e. $g_3 = g_4 = \ldots = 0$ in equation (2).

6.1 Stability maps

We show the behaviour of modes 1 and 2, based on $\Im(\Omega_1)$ and $\Im(\Omega_2)$ (with Ω_1 and Ω_2 calculated from equation (28)) and in the form of stability maps in the $L - A/\bar{U}$ plane (see Figures 2 and 3). We will consider a single control parameter, the burner length L, which ranges from 0.36 to 2.26 m; the amplitude $A/\bar{U}$ ranges from 0 to 0.31.

Figure 2 shows the case of the Rijke tube; on the left is the stability map of mode 1 in isolation, and on the right is that of mode 2 in isolation. Green areas indicate regions of instability: if the combustion system is such that the pair of values $(L,\ A/\bar{U})$ lie in an instability region, the mode will *grow* until $(L,\ A/\bar{U})$ reaches the border with the neighbouring stable region. White areas are regions of stability: if the point $(L,\ A/\bar{U})$ lies in such a region, the mode will *decay* in amplitude until the border with the next unstable region is reached. Interfaces between stable and unstable regions correspond to *limit cycles*: the growth rate of the mode is zero for values of $(L,\ A/\bar{U})$ along the interfaces (see also Bigongiari and Heckl[12]). Figure 3 shows equivalent stability maps for the quarter-wave resonator.

Each of the maps in Figures 2 and 3 represents the stability of a *single* mode in isolation. The overall stability of the combustion system is the result of the contribution of each mode and of the interaction between them, which is characterized by non-normality and nonlinearity.[24,25] The first step towards investigating the interaction between the first two modes of the combustor is to compare the growth rate of the two modes, so as to determine the dominant mode. This is shown in Figure 4: the green areas in the map indicate the regions where $\Im(\Omega_1) > \Im(\Omega_2)$.

From the maps in Figures 2 to 4, it is possible to deduce the nonlinear stability behaviour of the combustor. We illustrate this with two examples.

First, let us consider the Rijke tube of length $L = 1.2$ m. According to Figure 2, mode 2 is unstable at very low amplitudes, while mode 1 is stable. Hence we expect mode 2 to grow until its amplitude reaches the value $A/\bar{U} = 0.09$, which lies at the upper boundary of its unstable region (Figure 2(b)). At the point ($L = 1.2$ m, $A/\bar{U} = 0.09$), mode 1 is unstable (Figure 2(a)). We can therefore expect that mode 1 will now grow until it reaches the border of its unstable zone.

As a second example, let us consider a quarter-wave resonator of length $L = 2.0$ m. According to Figure 3, both modes are unstable at that point throughout the whole amplitude range. The comparative map in Figure 4(b) shows that mode 2 is the dominant one, and we therefore expect that an initial perturbation grows, with the dominant spectral component corresponding to mode 2.

In order to explore the nonlinear features of the two-mode interaction more rigorously, we will investigate the stability behaviour from the evolution of the overall acoustic velocity of the system.

6.2 Perturbation time histories

Following the numerical iteration method described in section 4.2, we calculate the time history of the perturbation $u_q(t)$ from its governing integral equation (21), combined with the local heat release rate (9) and amplitude-dependent parameters given by equations (15) to (17). The Green's function in the integral equation is evaluated from equation (2), where the sum includes the first two Green's function modes, $n = 1, 2$, but no higher modes. We present time histories for the two examples considered in the previous section.

The time history for the Rijke tube of length $L = 1.2$ m is displayed in Figure 5. It has been calculated by imposing the initial condition $u_q(t = 0)/\bar{U} = 0.01$.

The amplitude increases exponentially at first, then grows less rapidly; beyond about $t = 2$ s, a limit cycle is established with final amplitude $A/\bar{U} \simeq 0.1$. In order to check whether this time history is in line with the expectations based on the stability maps in Figure 2, we calculate the frequency spectrum for two time windows of the evolution: for [0, 1 s], i.e. for the early stage when the amplitude grows, and for [9 s, 10 s], i.e. after the limit cycle has established. The results are shown in Figure 6(a) and (b).

These spectra reveal that mode 1 is dominant during the growth stage of the evolution (small amplitudes), and that mode 2 takes over at the limit cycle stage (large amplitudes). This is not in agreement with the expectations based on the comparative map of Figure 4(a), in fact the opposite behaviour is predicted from the perturbation time history.

The time history for the quarter-wave resonator of length $L = 2$ m is displayed in Figure 7. Again, the initial condition was $u_q(t = 0)/\bar{U} = 0.01$.

The system is clearly stable, given that the initial perturbation decays to a smaller value. This is at variance with the predictions shown in the stability maps of Figure 3. Again, we investigate the evolution in more detail by calculating its frequency spectrum for two time windows: for the initial stage [0, 1 s], and for the later stage [9 s, 10 s]. The results are shown in Figure 8(a) and (b).

Mode 2 is dominant during the initial stage [0, 1 s] of the evolution (see Figure 8(a)). The amplitude of the perturbation decreases until saturation occurs for $A/\bar{U} \simeq 5 \times 10^{-4}$. This threshold, which is not visible in the comparative map of Figure 4(b), corresponds to the point where the first mode becomes dominant. The Fourier analysis of the acoustic velocity in the later time interval [9 s, 10 s] (see Figure 8(b)) confirms that the first mode is dominant after saturation.

These two examples show that a stability analysis in the frequency-domain cannot predict which of the modes will dominate the evolution, nor can it predict the final amplitude of the perturbation and the overall stability. In order to obtain this kind of information, it is necessary to calculate the time evolution of a perturbation and to examine its Fourier transform at different stages (or use other methods of time series analysis). This is in line with Moeck el al [9] who concluded from their frequency-domain analysis that the full dynamical picture can only be obtained from a time-domain analysis.

The failure of the modal stability analysis is not unexpected, given that non-normality and nonlinearity have been observed in the evolution of thermoacoustic instabilities (see e.g. Balasubramanian and Sujith,[24] Sujith et al.,[25] and Mariappan et al.[26]). In fact, the acoustic modes are modified by the thermoacoustic feedback; this has been demonstrated theoretically in Bigongiari and Heckl.[15] It has also been demonstrated experimentally in Mariappan et al.[26] that non-normality becomes more pronounced for increasing heater power.

In order to better illustrate the consequences of non-normal and nonlinear effects in the interaction between the modes, we perform a systematic investigation and calculate 1 s of time evolution for different values of L. The largest amplitude of u_q observed in this time-interval is plotted in Figure 9 as a function of L, spanning the range [0.36 m, 2.26 m] (the same as in section 6.1), with increment $\Delta L = 0.01$ m.

We observe that within certain ranges of L the perturbation amplitude grows to very large values. Juxtaposition with the comparative stability maps in Figure 4 reveals that these L-ranges correspond to the

L-ranges in which mode 2 is dominant (white regions in Figures 4(a) and (b)) for a large range of $A/\bar{U}$ values.

These results demonstrate that higher-order modes can play an important role in determining the overall stability behaviour. Having said that, we do not expect that a large number of modes are required for reliable stability predictions. This is because the contribution of higher-order modes becomes progressively negligible due to loss mechanisms (e.g. sound radiation from the combustor outlet) becoming more pronounced at higher frequencies.[27] Nevertheless this study highlights the nonlinear nature of the interaction between heat driven modes, and it shows that the role of higher-order modes cannot be neglected a *priori*.

7. Conclusions

In this paper, we have presented a fundamental study of the role of modal interaction in the occurrence and evolution of thermoacoustic instabilities. Our study is based on a Green's function approach, a method which is able to provide rapid stability predictions, while allowing an analysis of the key physical processes. We have analysed the interaction between the first and second acoustic mode in two ways: by calculating the time history of the perturbation where both modes are present, and by analysing the stability of each mode in isolation.

The time history of the perturbation has been calculated from an integral governing equation based on the Green's function of the system combined with a feedback model for the heat release law. This calculation shows the evolution of the perturbation resulting from the presence of two acoustic modes simultaneously.

A by-product of our Green's function approach is a frequency-domain method, where the stability behaviour of the individual modes is considered. This method is less powerful than our time-domain method (i.e. solving the integral governing equation): it cannot predict transient effects due to the nonlinear interaction between thermoacoustic modes.

This study represents a first step towards the modelling of nonlinearity and non-normality in combustion processes, based on a model which is able to describe the effects of thermoacoustic feedback on the acoustic modes as a function of key parameters.

Acknowledgement

The presented work is part of the Marie Curie Initial Training Network 'Thermoacoustic and aeroacoustic non-linearities in green combustors with orifice structures' (TANGO).

Declaration of Conflicting Interests

The author(s) declared no potential conflicts of interest with respect to the research, authorship, and/or publication of this article.

Funding

The author(s) disclosed receipt of the following financial support for the research, authorship, and/or publication of this article: We gratefully acknowledge the financial support from the European Commission under call FP7-PEOPLE-ITN-2012.

ORCID iD

Alessandra Bigongiari http://orcid.org/0000-0003-2401-5429

References

1. Scarinci T. Combustion instability and its passive control: Rolls-Royce aeroderivative engine experience. In: Lieuwen TC and Yang V (eds) *Combustion instabilities in gas turbine engines*. Reston: American Institute of Aeronautics and Astronautics, 2005, pp.65–88.
2. Goy CJ, James SR and Rea S. Monitoring combustion instabilities: E.ON UK's experience. In: Lieuwen TC and Yang V (eds) *Combustion instabilities in gas turbine engines*. Reston: American Institute of Aeronautics and Astronautics, 2005, pp.163–175.
3. Candel S. Combustion dynamics and control: progress and challenges. *Proc Combust Inst* 2002; 29: 1–28.
4. Lieuwen TC. Modeling premixed combustion–acoustic wave interactions: a review. *J Propul Power* 2003; 19: 765–781.
5. Huang Y and Yang V. Dynamics and stability of lean-premixed swirl-stabilized combustion. *Prog Energy Combust Sci* 2009; 35: 293–364.
6. Lieuwen TC and Yang V. *Combustion instabilities in gas turbine engines*. Reston: American Institute of Aeronautics and Astronautics, 2005.
7. Poinsot T and Veynante D. *Theoretical and numerical combustion*, 2nd ed. Philadelphia: Edwards, 2005.
8. Culick FEC. *Unsteady motions in combustion chambers for propulsion systems*. Research and Technology Organisation, 2006, NATO, RTO-AG-AVT-039.
9. Moeck JP and Paschereit CO. Nonlinear interactions of multiple linearly unstable thermoacoustic modes. *Int J of Spray and Combustion Dynamics* 2012; 4: 1–28.
10. Acharya V, Bothien M and Lieuwen T. Modal dynamics of thermoacoustic systems with closely-spaced eigenfrequencies. Proceedings of the International Symposium "Thermoacoustic Instabilities in Gas Turbines and Rocket Engines: Industry meets Academia", Munich, Germany, 30 May–2 June 2016, paper no. GTRE-042, pp.1–11.
11. Noiray N, Bothien M and Schuermans B. Investigation of azimuthal staging concepts in annular gas turbines. *Combustion Theory and Modelling* 2011; 15: 585–606.
12. Noiray N, Durox D, Schuller T, et al. Self-induced instabilities of premixed flames in a multiple injection configuration. *Combust Flame* 2006; 145: 435–446.
13. Noiray N, Durox D, Schuller T, et al. Passive control of combustion instabilities involving premixed flames anchored on perforated plates. *Proc Combust Inst* 2007; 31: 1283–1290.

14. Kashinath K, Hemchandra S and Juniper MP. Nonlinear phenomena in thermoacoustic systems with premixed flames. In: *Proceedings of the ASME Turbo Expo 2012*, Copenhagen, Denmark, 11–15 June 2012, paper no. 2012-68726.
15. Bigongiari A and Heckl M. A Green's function approach to the rapid prediction of thermoacoustic instabilities in combustors. *J Fluid Mech* 2016; 798: 970–996.
16. Komarek T and Polifke W. Impact of swirl fluctuations on the flame response of a perfectly premixed swirl burner. *J Eng Gas Turbines Power* 2010; 132: 061503-1,7.
17. Iurashev D, Campa G and Anisimov V. Response of swirl stabilized perfectly premixed flame to high-amplitude velocity excitations. In: *Proceedings of the 23rd international Congress on Sound and Vibration*, Athens, Greece, 10–14 July 2016.
18. Bigongiari A and Heckl M. A Green's function approach to the study of hysteresis in a Rijke tube. In: *Proceedings of the 23nd international Congress on Sound and Vibration*, Athens, Greece, 10–14 July 2016.
19. Bigongiari A and Heckl M. A Green's function approach to the study of hysteresis in a Rijke tube. In: *Proceedings of the 24th international Congress on Sound and Vibration*, London, UK, 23–27 July 2017.
20. Gopinathan SM, Iurashev D, Bigongiari A and Heckl M. Nonlinear analytical flame models with amplitude-dependent time-lag distributions. *Int J of Spray and Combustion Dynamics*. DOI: 10.1177/1756827717728056.
21. Noiray N, Durox D, Schuller T, et al. A unified framework for nonlinear combustion instability analysis based on the flame describing function. *J Fluid Mech* 2008; 615: 139–167.
22. Stow SR and Dowling AP. A time-domain network model for nonlinear thermoacoustic oscillations. *J Eng Gas Turbines Power* 2009; 131, article no 03150.
23. Heckl MA and Howe MS. Stability analysis of the Rijke tube with a Green's function approach. *J Sound Vib* 2007; 305: 672–688.
24. Balasubramanian K and Sujith RI. Thermoacoustic instability in a Rijke tube: non-normality and nonlinearity. *Phys Fluids* 2008; 20: 004103.
25. Sujith RI, Juniper MP and Schmid PJ. Non-normality and nonlinearity in thermoacoustic instabilities. *Int J Spray Combust Dynam* 2016; 8: 119–146.
26. Mariappan S, Sujith RI and Schmid PJ. Experimental investigation of non-normality and transient growth in thermoacoustic instabilities. In: *47th AIAA/ASME/SAE/ASEE Joint Propulsion Conference and Exhibit*, San Diego, CA, 31 July–3 August 2011.
27. Silva F, Guillemain P, Kergomard J, Mallaroni B and Norris AN. Approximation formulae for the acoustic radiation impedance of a cylindrical pipe. *J Sound Vib* 2009; 322: 255–263.